Available online at www.sciencedirect.com

ScienceDirect

International Journal of Solids and Structures 44 (2007) 7938–7954

INTERNATIONAL JOURNAL OF SOLIDS AND STRUCTURES

www.elsevier.com/locate/ijsolstr

Modeling and validation of the large deformation inelastic response of amorphous polymers over a wide range of temperatures and strain rates

J. Richeton [a,1], S. Ahzi [a,*], K.S. Vecchio [b], F.C. Jiang [b], A. Makradi [a]

[a] *Institut de Mécanique des Fluides et des Solides—UMR 7507, Université Louis Pasteur/CNRS, 67000 Strasbourg, France*
[b] *Materials Science and Engineering Program, University of California San Diego, La Jolla, CA 92093-0411, USA*

Received 4 December 2006; received in revised form 19 May 2007
Available online 31 May 2007

Abstract

A robust physically consistent three-dimensional constitutive model is developed to describe the finite mechanical response of amorphous polymers over a wide range of temperatures and strain rates, including the rubbery region and for impact loading rates. This thermomechanical model is based on an elastic–viscoplastic rheological approach, wherein the effects of temperature, strain rate, and hydrostatic pressure are accounted for. Intramolecular, as well as intermolecular, interactions under large elastic–inelastic behavior are considered for the mechanisms of deformation and hardening. For a wide range of temperatures and strain rates, our simulated results for poly(methyl methacrylate) (PMMA) and polycarbonate (PC) are in good agreement with experimental observations.

Keywords: Modeling; Amorphous polymers; Temperature and rate effects; Impact loading rates

1. Introduction

Polymer-based materials represent the largest and fastest growing area of materials for engineering applications. Due to their unique combination of properties, such as lightweight or ease of processing, polymers have transformed the quality of our everyday life. For many applications, an accurate knowledge of the mechanical behavior of these materials is of prime importance to improve performance and increase efficient use. Consequently, the ability of predicting the mechanical behavior of polymers is a strong motivation for the mathematical modeling of the elastic–inelastic deformation of these materials.

Through several decades, many physically based models have been introduced to account for the mechanisms of deformation of amorphous polymers. The elementary mechanisms are identified as thermally

* Corresponding author. Tel.: +33 390 242952; fax: +33 388 614300.
E-mail address: ahzi@imfs.u-strasbg.fr (S. Ahzi).
[1] Presently working for Momentive Performance Materials, Leverkusen, Germany.

0020-7683/$ - see front matter
doi:10.1016/j.ijsolstr.2007.05.018

activated processes of molecular movements. This is the case for the state transition theory of Eyring (1936), the conformational change theory of Robertson (1966) and the intermolecular shear resistance model of Argon (1973). However, as it was discussed by Richeton et al. (2003), the use of these latter models has to be restricted to a specific domain of temperatures and strain rates. Among other works, a great deal of attention has been given by Bauwens, Bauwens-Crowet, and co-workers to the yield stress of amorphous polymers (Bauwens et al., 1969; Bauwens, 1972; Bauwens-Crowet et al., 1969, 1972; Bauwens-Crowet, 1973). In their work, these authors have introduced two rheological processes, α and β, to describe the yield behavior on a wide range of temperatures and strain rates. For five glassy polymers, they showed that the rheological β process corresponds to a well-defined molecular process, the secondary relaxation of polymer chains. They also mentioned that, in their theory, there is no connection between the rheological α process with any other identified molecular relaxation of polymer chains (such as the glass transition).

Most of the pre-cited models can be employed to predict the yield behavior of amorphous polymers, but they are also frequently part of a more complex deformation theory where they are used as a rate dependent plasticity model acting in parallel with a network model to account for the alignment of polymer chains with deformation (Boyce et al., 1988; Arruda and Boyce, 1993; Arruda et al., 1995). More recently, Mulliken and Boyce (2006) employed the model of Bauwens and Bauwens-Crowet (Bauwens et al., 1969; Bauwens, 1972; Bauwens-Crowet et al., 1969, 1972; Bauwens-Crowet, 1973) to describe the mechanical response of amorphous polymers at high strain rates for various temperatures. However, the constitutive model of Mulliken and Boyce (2006) lacks robustness since their flow rule is not valid through the glass transition region. In fact, the adiabatic heating developed under dynamic loading leads to drastic increase of temperature in the material which may trigger a change from the glassy to the rubbery state.

Therefore, due to the limitations of the existing models, we propose here a robust, physically consistent, three-dimensional constitutive model for the mechanical response of amorphous polymers. This thermomechanical model is designed to be valid on a wide range of temperatures and strain rates, including the rubbery region and for impact loading rates. This model also accounts for the possible change from the glassy to the rubbery state in case of strong local adiabatic heating (Bjerke and Lambros, 2002; Bjerke et al., 2002).

Our present contribution is organized as follows. In Section 2, we will introduce the different constitutive equations such as our new formulation of the cooperative model for the yield stress of amorphous polymers, the 8-chain model of Arruda and Boyce (1993), or the temperature dependence of the material properties. Next, the kinematics theory of finite strains as well as the numerical implementation of the thermomechanical model are briefly reviewed in Section 3. With poly(methyl methacrylate) (PMMA) and polycarbonate (PC) as reference materials, Section 4 is a discussion on the attributes of the new robust constitutive model. Our simulated results are furthermore compared to experimental results for a wide range of temperatures and strain rates.

2. Model formulation

Technologically advanced applications of polymers require development of physically consistent models that are able to describe the temperature and strain rate dependence of the mechanical response of these materials. The constitutive model considered in this work is developed after physical considerations by using a molecular theory for the plastic flow and an orientational model for the deformation of polymer chains at large strains. Fig. 1 shows the schematic representation of the elastic–viscoplastic constitutive model. At small deformations, the polymer is assumed to behave elastically and Hooke's law is used to predict the mechanical response. At yield, the polymer chains overcome the isotropic resistance due to plastic flow, which acts in parallel with the anisotropic resistance due to molecular chain alignment. The details of temperature and strain rate dependence of the constitutive equations describing the large deformation of amorphous polymer are outlined in the following sections.

2.1. Flow rule

Most of the existing theories for the yield stress of amorphous polymers can be used only in specific domains of temperature and/or strain rate. By taking into account the influence of the secondary relaxation

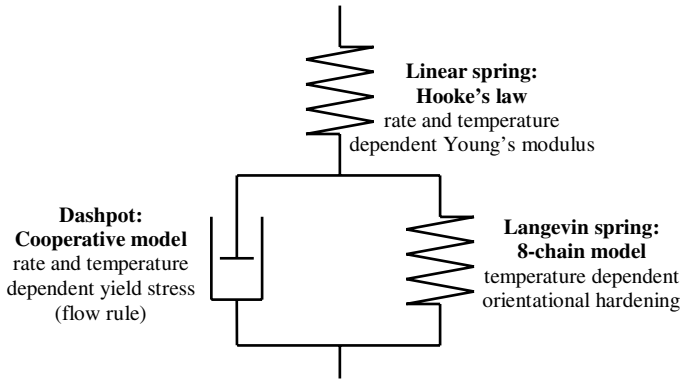

Fig. 1. Schematic representation of the mechanical model.

of polymer chains, a new formulation of the cooperative model of Fotheringham and Cherry (1976) for the yield response of amorphous polymers has shown a good agreement with experimental results over a wide range of strain rates and temperatures, including the glass transition region and impact loading rates (Richeton et al., 2005a, 2006).

2.1.1. Flow rule below the glass transition

For the yield behavior of amorphous polymers, the plastic shear strain rate, $\dot{\gamma}_p$, is expressed by the cooperative model as

$$\dot{\gamma}_p = \dot{\gamma}_0 \exp\left(-\frac{\Delta H_\beta}{k\theta}\right) \sinh^n\left(\frac{(\tau - t_i)\cdot V}{2k\theta}\right) \tag{1}$$

where $\dot{\gamma}_0$ is the pre-exponential shear rate factor, ΔH_β is the activation energy of the secondary relaxation of polymer chains, k is Boltzmann's constant, θ is the absolute temperature, n is a material parameter describing the cooperative nature of the polymer chain segments, V is the shear activation volume, τ is the effective equivalent shear stress, and t_i is the evolving internal shear stress. The internal shear stress evolves significantly from its initial value to account for the strain softening. We would like to point out that at the yield point, $t_i = \tau_i$, where τ_i is the initial test condition value of the internal shear stress defined by

$$\tau_i = \tau_i(0) - m\cdot\theta + \alpha_p \cdot P \tag{2}$$

where $\tau_i(0)$ is the internal shear stress at the temperature $\theta = 0$ K, and m is a material parameter roughly equal to $\tau_i(0)/T_g$, T_g being the glass transition temperature. The parameter α_p is the hydrostatic pressure coefficient and P is the hydrostatic pressure. Eq. (2) is the classical form of the internal shear stress, where τ_i presents a linear decrease with temperature. This formulation allows us to account for the differences in the mechanical response of the polymer associated with the temperature and pressure effects. For further details on the physics of the cooperative model, the reader may refer to the work of Richeton et al. (2005a, in press).

2.1.2. Flow rule through the glass transition

In line with the free-volume theory of William et al. (1955), the plastic shear rate, $\dot{\gamma}_p$, is given through the glass transition by (Richeton et al., 2005a):

$$\dot{\gamma}_p = \dot{\gamma}_0 \exp\left(-\frac{\Delta H_\beta}{k\theta}\right) \exp\left(\frac{\ln 10 \times c_1^g \cdot (\theta - T_g)}{c_2^g + \theta - T_g}\right) \sinh^n\left(\frac{\tau \cdot V}{2k\theta}\right) \tag{3}$$

where c_1^g and c_2^g are the WLF parameters relative to T_g. It should be noted that above T_g, the internal stresses τ_i and t_i are taken to be zero as strain softening vanishes in the rubbery state.

In this study, the parameters of the cooperative model were determined from previous work concerning uniaxial compression tests (Richeton et al., 2006). Given that the implementation of the flow rule is generally made in terms of shear (Boyce et al., 1988), a correction of the model's parameter has to be introduced. This

correction is based on the von Mises relationship taking into account the effect of the hydrostatic pressure. The pre-exponential shear rate factor, $\dot{\gamma}_0$, can be expressed as a function of Poisson's ratio, υ, and of the pre-exponential rate factor, $\dot{\varepsilon}_0$: $\dot{\gamma}_0 = (2\sqrt{3}/3)(1+\upsilon)\dot{\varepsilon}_0 \approx \sqrt{3}\dot{\varepsilon}_0$. The correction of the activation volume and stress parameters given for uniaxial compression results in the following equations:

$$\begin{cases} \tau_i(0) = \dfrac{(1-\alpha_p/3)}{\sqrt{3}}\sigma_i(0) \\ m^{\text{shear}} = \dfrac{(1-\alpha_p/3)}{\sqrt{3}} m^{\text{compression}} \\ V^{\text{shear}} = \dfrac{\sqrt{3}}{1-\alpha_p/3} V^{\text{compression}} \end{cases} \tag{4}$$

The shear parameters used for the implementation of the cooperative model are given in Table 1.

2.2. Strain softening

The evolution of the shear internal resistance, t_i, of the cooperative model follows closely the work of Boyce et al. (1988). The internal stress decreases with plastic deformation until reaching a preferred structural state. Indeed, after yielding, it can be assumed that molecular defects rearrange themselves until reaching a more stable configuration. A phenomenological evolution of the internal stress during strain softening is described by

$$\dot{t}_i = h \cdot \left(1 - \frac{t_i}{\tau_{ps}}\right) \cdot \dot{\gamma}_p \tag{5}$$

where h is the softening slope and τ_{ps} is the stress referring to the preferred structural state of the material. The stress, τ_{ps}, may depend on temperature and strain rate. Concerning our modeling, we assume that the ratio τ_{ps}/τ_i is constant. Here, we remind the reader that τ_i is the initial value of the internal stress, where $\tau_i = \tau_i(0) - m \cdot \theta + \alpha_p \cdot P$. As a consequence, we note that τ_{ps} is only temperature dependent and that the model does not predict any strain softening for $\theta \geqslant T_g$ since the internal stress is zero. The softening parameters related to Eq. (5) are given in Table 1.

2.3. Orientational hardening

Once a polymer is stressed to the point of overcoming the intermolecular resistance, the chains begin to orient themselves. The resistance to plastic flow due to the molecular alignment could be described by the 8-chain model of Arruda and Boyce (1993). The principal components of the network stress tensor are expressed as

Table 1
Parameters for the flow rule and the strain softening

	PMMA	PC
n	6.37	5.88
V (m^3)	9.75×10^{-29}	9.18×10^{-29}
$\tau_i(0)$ (MPa)	100	81
m (MPa/K)	0.25	0.14
$\dot{\gamma}_0$ (s^{-1})	1.16×10^{16}	1.36×10^{13}
ΔH_β (kJ/mol)	90	40
c_1^g	32.58	16.19
c_2^g (°C or K)	83.5	55.6
α_p	0.26	0.08
τ_{ps}/τ_i	0.20	0.57
h (MPa/K)	30	300

$$B_i = C_R(\theta)\frac{\sqrt{N(\theta)}}{3}\mathcal{L}^{-1}\left(\frac{\lambda_{chain}}{\sqrt{N(\theta)}}\right)\frac{\lambda_i^2-\lambda_{chain}^2}{\lambda_{chain}}, \quad i=1,2,3 \tag{6}$$

where $C_R(\theta)$ is the rubbery modulus, $N(\theta)$ is the number of rigid chain links between entanglements, λ_i are the principal components of the plastic stretch tensor, $\mathbf{V}^p$, which is the symmetric part of the plastic deformation gradient, $\mathbf{F}^p$. The values λ_i^2 are the eigenvalues of the tensor $(\mathbf{V}^p)^2 = \mathbf{F}^p(\mathbf{F}^p)^T$, $(\mathbf{F}^p)^T$ being the transpose of $\mathbf{F}^p$. The inverse Langevin function, $\mathcal{L}^{-1}$, is calculated using the Padé approximation of Cohen (1991), $\mathcal{L}^{-1}(x) \approx x\cdot(3-x^2)/(1-x^2)$. In what follows, we will compare two approaches for the temperature dependence of $C_R(\theta)$ and $N(\theta)$ since the mechanical properties of polymers are known to be strongly affected by temperature.

2.3.1. Dissociating network description

The temperature dependence of the rubbery modulus, $C_R(\theta)$, proposed by Arruda et al. (1995) is taken to be proportional to the chain density, $n(\theta)$:

$$C_R(\theta) = n(\theta)k\theta \tag{7}$$

where the thermally evolving chain density, $n(\theta)$, is function of a thermal dissociation energy, E_a, and also parameters representing the non-dissociating, A, and the dissociating, B, network parts:

$$n(\theta) = A - B\cdot\exp\left(\frac{-E_a}{k\theta}\right) \tag{8}$$

The thermally evolving chain density, $n(\theta)$, for which a chain is statically defined as the segment between physical entanglements results in an evolution of the number of statistically rigid links per chain, $N(\theta)$. In fact, the decrease in entanglement incidences, $n(\theta)$, with increasing temperature, results in an increase in the average number of links per chain, $N(\theta)$, according to the following relationship:

$$n(\theta)\cdot N(\theta) = \text{constant} \tag{9}$$

The total number of rigid links in the model and hence, the mass of the physical system, is conserved. Consequently, the thermally evolving number of statistical rigid links per chain is given by

$$N(\theta) = \frac{n(298\ \text{K})\cdot N(298\ \text{K})}{A - B\cdot\exp(-E_a/k\theta)} \tag{10}$$

where $n(298\ \text{K})$ and $N(298\ \text{K})$ refer to the room temperature $\theta = 298\ \text{K}$.

2.3.2. Linear phenomenological description

In line with the experimental results of Meyer and Ferri (1935) concerning the temperature dependence of the elastic stress of rubbery materials, we proposed a linear phenomenological model for the dependence on temperature of the material parameters $C_R(\theta)$ and $N(\theta)$. The experimental stress–temperature curve (see Fig. 2) for a rubber presents a linear behavior over a large range of temperatures. The rubber elastic stress increases linearly above the glass temperature ($T_g = 215\ \text{K}$), which is in agreement with the prediction of the finite strain elasticity theories (i.e. $C_R = n(\theta)k\theta$). While below the glass transition temperature the

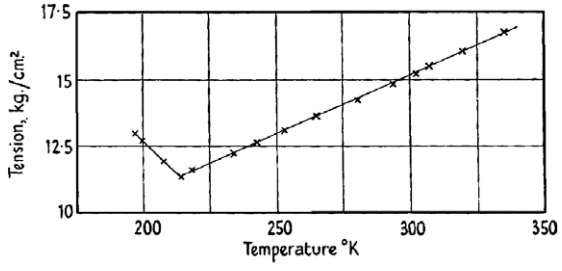

Fig. 2. Stress of a rubber at constant length as a function of absolute temperature. After Meyer and Ferri (1935).

stress–temperature curve shows an inversion of the sign of the curve's slope. In the glassy state, the internal energy of the rubber is more predominant than the entropic term. In accordance with these experimental observations, we have expressed the temperature dependence of the rubbery modulus, $C_R(\theta)$, as follows:

$$\begin{cases} C_R(\theta \leqslant T_g) = C_R(0) - a \cdot \theta \\ C_R(\theta \geqslant T_g) = \dfrac{C_R(0) - a \cdot T_g}{T_g} \cdot \theta \end{cases} \tag{11}$$

where $C_R(0)$ and a are material parameters. For the temperature dependence of the number of rigid links between entanglements, $N(\theta)$, we propose the following phenomenological description:

$$\begin{cases} N(\theta \leqslant T_g) = N(0) + b \cdot \theta \\ N(\theta \geqslant T_g) = N(0) + b \cdot T_g \end{cases} \tag{12}$$

where $N(0)$ and b are material parameters. The expression of $N(\theta)$ is obtained by the fact that below T_g, the orientational hardening should decrease with increasing temperature. For a given strain, an increase of $N(\theta)$ will decrease the orientational hardening. The linear dependence of $N(\theta)$ with temperature is a very rough estimate. We used this description to avoid any major contradiction with the experimental results of Meyer and Ferri (1935). While above T_g, the expression of $N(\theta)$ is built on the following two assumptions: (1) $N(\theta)$ is a continuous function through T_g, (2) $N(\theta)$ is constant above T_g, according to the experimental results of G'Sell and Souami (1997). Indeed, these authors noticed that strain hardening decreases gradually with temperature in the glassy state, but keep a significant value in the rubbery state.

2.3.3. Comparison between the two formulations

The comparison between the two formulations is made for PMMA. The parameters used for the temperature dependence of the strain hardening can be found in Table 2. Fig. 3 reports the temperature dependence of the hardening modulus, $C_R(\theta)$. The temperature dependence suggested by Arruda et al. (1995) predicts the opposite phenomenon from that experimentally observed by Meyer and Ferri (1935) and by G'Sell and Souami (1997). Further, due to a numerical artifact, the inflexion point in their curve does not occur for the glass transition. We believe that the temperature dependence model of Arruda et al. (1995) for the orientational hardening is only valid within a small range of temperatures. As mentioned by Meyer and Ferri (1935), the hardening modulus has to decrease with temperature for $\theta < T_g$ since the internal energy term is far superior compared to the entropic term.

Fig. 4 reports the predicted temperature dependence of the number of rigid links between entanglements of Arruda et al. (1995) compared to our approach. The temperature dependence model proposed by Arruda et al. (1995) predicts a drastic increase in the number of rigid links in the vicinity of the glass temperature transition. This implies that the orientational hardening should tend to zero in this region, which is in contradiction with the experimental results of G'Sell and Souami (1997).

The good fit of experimental stress–strain curves, obtained by Arruda et al. (1995), might be explained by the competition between orientational hardening and strain softening. The orientational hardening can be numerically compensated with the strain softening for good description of the stress–strain response. Concerning our phenomenological formulation for the temperature dependence of the orientational hardening, we have to mention that our approach is also certainly far from the real behavior of the polymer chains. As it is also the case with Arruda et al. (1995), the values taken by N are typically in the order of 2–4. These values

Table 2
Parameters for the phenomenological temperature dependence of the orientational hardening

	PMMA	PC
$C_R(0)$ (MPa)	91.15	37.57
a (MPa/K)	0.226	0.077
$N(0)$	1.515	1.960
b (1/K)	0.0025	0.0013

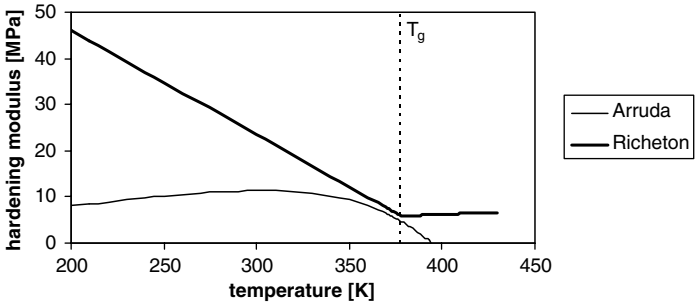

Fig. 3. Temperature dependence of the hardening modulus for PMMA.

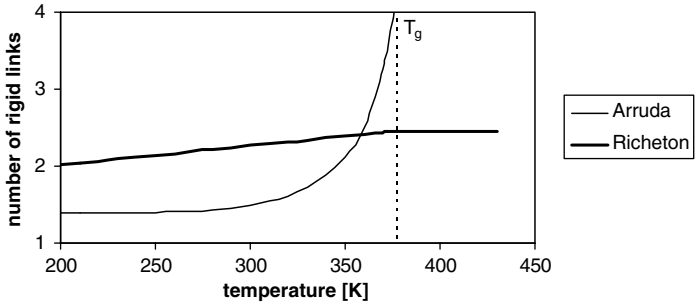

Fig. 4. Temperature dependence of the number of rigid links between entanglements for PMMA.

are much too small to be an actual number of statistical links between the entanglements of a physically cross-linked system. As described by Dooling et al. (2002), a more physical description can be obtained via the slip-links/cross-links model of Edwards and Vilgis (1986). However, as stated by Sweeney (1999), the use of the 8-chain model is convenient to use from a mathematical point view and it presents very few differences with the model of Edwards and Vilgis (1986) in regards to the fitting of data.

2.4. Modeling the effects of temperature and strain rate for Young's modulus

It is well established that Young's modulus of polymers is strongly influenced by temperature and strain rate. For the high strain rates, typical experimental data could be found in the literature (see for instance Cady et al., 2003). In line with these observations, we have recently modified the temperature dependent statistical model for the stiffness modulus of Mahieux and Reifsnider (2001, 2002) into a robust constitutive model, which considers the effect of strain rate as well (Richeton et al., 2005b). Mahieux and Reifsnider (2001, 2002) used Weibull statistics to represent the failure of secondary bonds (e.g. van der Waals, polar attraction) during the different relaxation processes that lead to stiffness modulus change with temperature. In the case of amorphous polymers, it is assumed that the material undergoes three main transitions (β relaxation, glass transition and flow) characterized by the associated transition temperatures (T_β, T_g, and T_f). The temperature and strain rate dependence of Young's modulus is then given by

$$E(\theta,\dot{\varepsilon}) = (E_1(\dot{\varepsilon}) - E_2(\dot{\varepsilon}))\cdot\exp\left(-\left(\frac{\theta}{T_\beta(\dot{\varepsilon})}\right)^{m_1}\right) + (E_2(\dot{\varepsilon}) - E_3(\dot{\varepsilon}))\cdot\exp\left(-\left(\frac{\theta}{T_g(\dot{\varepsilon})}\right)^{m_2}\right) + E_3(\dot{\varepsilon})\cdot\exp\left(-\left(\frac{\theta}{T_f(\dot{\varepsilon})}\right)^{m_3}\right) \tag{13}$$

where the moduli, $E_i(\dot{\varepsilon})$, are the instantaneous stiffness of the material at the beginning of each transition region, and the parameters, m_i, are the Weibull moduli corresponding to the statistics of the bond breakage. The

strain rate dependence of the transition temperatures and instantaneous stiffness was discussed by Richeton et al. (2005b) according to physical considerations

$$\begin{cases} E_i = E_i^{\mathrm{ref}} \cdot (1 + s \cdot \log(\dot{\varepsilon}/\dot{\varepsilon}^{\mathrm{ref}})) \\ \dfrac{1}{T_\beta} = \dfrac{1}{T_\beta^{\mathrm{ref}}} + \dfrac{k}{\Delta H_\beta} \ln(\dot{\varepsilon}^{\mathrm{ref}}/\dot{\varepsilon}) \\ T_g = T_g^{\mathrm{ref}} + \dfrac{-c_2^g \cdot \log(\dot{\varepsilon}^{\mathrm{ref}}/\dot{\varepsilon})}{c_1^g + \log(\dot{\varepsilon}^{\mathrm{ref}}/\dot{\varepsilon})} \\ T_f = T_f^{\mathrm{ref}} \cdot (1 + 0.01 \cdot \log(\dot{\varepsilon}/\dot{\varepsilon}^{\mathrm{ref}})) \end{cases} \tag{14}$$

where E_i^{ref} are the instantaneous stiffness at a chosen reference strain rate, $\dot{\varepsilon}^{\mathrm{ref}}$, and s is the sensitivity of the modulus to strain rate. The use of a logarithm function was driven by the fact that mechanical properties of polymer systems are usually sensitive to the logarithm of the rate of loading. Regarding the transition temperatures (T_β, T_g, and T_f), we postulated that: (1) the β movements are activated by an Arrhenius process, (2) the glass transition is described by the free-volume theory of William et al. (1955), and (3) a phenomenological dependence can be used to depict the rate dependence of the flow temperature, $T_f(\dot{\varepsilon})$, where the value of 0.01 was arbitrary chosen. The parameters for the temperature and rate dependence of the stiffness modulus of PMMA and PC are given in Table 3.

2.5. Influence of temperature on the material properties

The physical properties of polymers are known to be strongly altered by temperature and in particular by the glass transition. In the books of Van Krevelen (1990) and Bicerano (1993), some empirical and semi-empirical formulae can be found to determine the temperature dependence of material properties as a function of the material properties at 298 K. Hence, the temperature dependence of the density, $\rho(\theta)$, is expressed by

$$\begin{cases} \rho(\theta \leqslant T_g) = \rho(298\ \mathrm{K}) \cdot \dfrac{(1.42 T_g + 44.7)}{(1.42 T_g + 0.15 \cdot \theta)} \\ \rho(\theta \geqslant T_g) = \rho(298\ \mathrm{K}) \cdot \dfrac{(1.42 T_g + 44.7)}{(1.27 T_g + 0.30 \cdot \theta)} \end{cases} \tag{15}$$

The temperature dependence of the thermal conductivity, $\Gamma(\theta)$, is given by

$$\begin{cases} \Gamma(\theta \leqslant T_g) = \Gamma(T_g) \cdot \left(\dfrac{\theta}{T_g}\right)^{0.22} \\ \Gamma(\theta \geqslant T_g) = \Gamma(T_g) \cdot \left(1.2 - 0.2 \dfrac{\theta}{T_g}\right) \end{cases} \tag{16}$$

Table 3
Parameters for the modeling of Young's modulus of PMMA and PC

	PMMA	PC
$\dot{\varepsilon}^{\mathrm{ref}}$ (s^{-1})	1	1
E_1^{ref} (MPa)	5100	3500
E_2^{ref} (MPa)	2700	1700
E_3^{ref} (MPa)	20	20
T_β^{ref} (K)	290	195
T_g^{ref} (K)	387	423
T_f^{ref} (K)	466	436
m_1	5	5
m_2	40	80
m_3	20	15
s	0.087	0.011

The influence of hydrostatic pressure on the modulus is neglected in this study.

Table 4
Material properties at 298 K

	PMMA	PC
ρ(298 K) (kg/m^3)	1190	1200
Γ(298 K) (W/m K)	0.190	0.187
c_p^s(298 K) (J/kg K)	1370	1200
c_p^l(298 K) (J/kg K)	1835	1615
β(298 K) (m/m K)	80.0×10^{-6}	70.2×10^{-6}
ν(298 K)	0.35	0.36

with $\Gamma(T_g) = \Gamma(298\text{ K})\cdot(\frac{T_g}{298})^{0.22}$. The temperature dependence of the heat capacity, $c_p(\theta)$, is given by

$$\begin{cases} c_p(\theta < T_g) = c_p^s(298\text{ K})\cdot(0.106 + 3.0\cdot10^{-3}\cdot\theta) \\ c_p(\theta \geqslant T_g) = c_p^l(298\text{ K})\cdot(0.613 + 1.3\cdot10^{-3}\cdot\theta) \end{cases} \tag{17}$$

where the parameters $c_p^s(298\text{ K})$ and $c_p^l(298\text{ K})$ are the heat capacities of solid and liquid polymers at 298 K.

The temperature dependence of the coefficient of linear thermal expansion, $\beta(\theta)$, is given by

$$\begin{cases} \beta(\theta < T_g) = \beta(298\text{ K}) \\ \beta(\theta \geqslant T_g) = \beta(298\text{ K}) + \frac{0.113}{3T_g} \end{cases} \tag{18}$$

The temperature dependence of Poisson's ratio, $\nu(\theta)$, is given by

$$\begin{cases} \nu(\theta < T_g) = \nu(298\text{ K}) \\ \nu(\theta \geqslant T_g) = 0.499 \end{cases} \tag{19}$$

All the parameters required for Eqs. (15)–(19) are given in Table 4.

2.6. Indication for the determination of the model parameters

Most model parameters are material constants that could be obtained from basic physical properties. But other parameters have to be determined by fitting experimental results. Information on the different identification procedures can be found in the literature. The parameters for the flow rule were determined by a technique exposed in a previous work (Richeton et al., 2006). The determination of the parameters for Young's modulus is also described in another work (Richeton et al., 2005b). Concerning the identification of the remaining parameters, the reader may consult the work of Boyce et al. (1988) for full details. Once the hardening parameters, $C_R(\theta)$ and $N(\theta)$, are known for different temperatures, their temperature dependence is obtained from a linear regression according to Eqs. (11) and (12).

3. Three-dimensional constitutive model

3.1. Kinematics of finite strain

As it is generally the case in mechanics of rubber and plastics, finite deformation tensors are used for large deformations. In what follows, we briefly address the kinematics of finite deformation, since the full details can be found elsewhere (Boyce et al., 1988, 1992; Arruda et al., 1995).

The deformation of a material from its initial isotropic reference state, $\Omega_0(\theta_0)$, at a temperature θ_0 to an actual state $\Omega_t(\theta)$ is described by the gradient of deformation, $\mathbf{F}$. This tensor is multiplicatively decomposed into elastic, $\mathbf{F}^e$, thermal, $\mathbf{F}^{th}$, and plastic, $\mathbf{F}^p$, components:

$$\mathbf{F} = \mathbf{F}^e\mathbf{F}^{th}\mathbf{F}^p \tag{20}$$

This decomposition considers a conceptual sequence of unloading steps. A material point, $d\Omega_t(\theta)$, is first isothermally unloaded to a stress state via $\mathbf{F}^{e-1}$ to a local intermediate configuration $d\overline{\Omega}_t(\theta)$. The material point is then taken to undergo a reversible heat transfer process whereby its temperature changes from θ to θ_0 via $\mathbf{F}^{th-1}$ to a second unloaded intermediate configuration $d\overline{\Omega}_t(\theta_0)$.

The deformation gradient tensors can be further decomposed according to a polar decomposition. For instance, $\mathbf{F}^e$ may be decomposed in terms of the elastic stretch tensors, $\mathbf{V}^e$ or $\mathbf{U}^e$ (left or right, respectively), and the elastic rotation tensor, $\mathbf{R}^e$:

$$\mathbf{F}^e = \mathbf{V}^e\mathbf{R}^e = \mathbf{R}^e\mathbf{U}^e \tag{21}$$

The velocity gradient, $\mathbf{L}$, is then obtained by differentiating the product decomposition as

$$\mathbf{L} = \dot{\mathbf{F}}\mathbf{F}^{-1} = \mathbf{L}^e + \mathbf{F}^e[\mathbf{L}^{th} + \mathbf{F}^{th}\mathbf{L}^p\mathbf{F}^{th-1}]\mathbf{F}^{e-1} \tag{22}$$

where the elastic, thermal, and plastic velocity gradients are given by

$$\begin{cases} \mathbf{L}^e = \dot{\mathbf{F}}^e\mathbf{F}^{e-1} \\ \mathbf{L}^{th} = \dot{\mathbf{F}}^{th}\mathbf{F}^{th-1} \\ \mathbf{L}^p = \dot{\mathbf{F}}^p\mathbf{F}^{p-1} \end{cases} \tag{23}$$

The velocity gradient of the $d\overline{\Omega}_t(\theta)$ configuration is given by

$$\mathbf{L}^{thp} = \dot{\mathbf{F}}^{thp}\mathbf{F}^{thp-1} = \mathbf{L}^{thp} + \mathbf{F}^{th}\mathbf{L}^p\mathbf{F}^{th-1} \tag{24}$$

Further, the velocity gradient may be decomposed as the sum of the symmetric stretching tensor, $\mathbf{D}^{thp}$, and the skew-symmetric spin tensor, $\mathbf{W}^{thp}$:

$$\mathbf{L}^{thp} = \mathbf{D}^{thp} + \mathbf{W}^{thp} \tag{25}$$

For convenience and numerical efficiency, $\mathbf{W}^{thp}$ is frequently set to zero. The rate of deformation, $\mathbf{D}^{thp}$, may be further decomposed into a plastic stretching, $\overline{\mathbf{D}}^p$, and a thermally induced stretching, $\beta(\theta)\cdot\dot{\theta}\cdot\mathbf{I}$, where $\beta(\theta)$ is the temperature dependent linear thermal expansion coefficient:

$$\mathbf{D}^{thp} = \overline{\mathbf{D}}^p + \beta(\theta)\dot{\theta}\mathbf{I} \tag{26}$$

According to Boyce et al. (1988), the thermal expansion tensor can be taken to be isotropic. Concerning the plastic stretching tensor, $\overline{\mathbf{D}}^p$, a thermodynamic formalism by Parks et al. (1984) suggested a flow rule specified by the applied plastic shear strain rate, $\dot{\gamma}_p$:

$$\overline{\mathbf{D}}^p = \frac{\dot{\gamma}_p}{\sqrt{2}\tau}\overline{\mathbf{T}}^{*\prime} \tag{27}$$

In Eq. (27), $\overline{\mathbf{T}}^{*\prime}$ is the deviatoric part of the driving stress tensor expressed in $\overline{\Omega}_t(\theta)$:

$$\overline{\mathbf{T}}^{*} = \mathbf{R}^{eT}\mathbf{T}\mathbf{R}^e - \mathbf{B} \tag{28}$$

Here, $\mathbf{R}^e$ has been defined in Eq. (21) and $\mathbf{T}$ is the Cauchy stress given by

$$\mathbf{T} = \frac{1}{J}\mathbf{C}^e\ln(\mathbf{V}^e) \tag{29}$$

where J is the volume change given by $\det(\mathbf{F}^e)$ and $\mathbf{C}^e$ is the temperature dependent isotropic elastic modulus tensor. The rate and temperature dependences of Young's modulus were given in Section 2.4.

In Eq. (28), $\mathbf{B}$ is the back stress tensor. Its principal components are defined by Eq. (6), where the λ values are the principal components of the left plastic stretch tensor, $\mathbf{V}^p$. In Eq. (27), τ is the effective equivalent stress defined by

$$\tau = \left[\frac{1}{2}\overline{\mathbf{T}}^{*\prime}\cdot\overline{\mathbf{T}}^{*\prime}\right]^{1/2} \tag{30}$$

$\overline{\mathbf{T}}^{*}$ is referred to as the driving stress tensor since it is only this portion of the stress that continues to activate plastic flow.

At time zero, the deformation gradient tensors, $\mathbf{F}$, $\mathbf{F}^{e}$, $\mathbf{F}^{th}$, and $\mathbf{F}^{p}$, are all unit tensor, $\mathbf{I}$. The stress and strain of the material are zero. The velocity gradient, $\mathbf{L}$, is given as a deformation constraint. At each increment, the equivalent stress and the equivalent strain were calculated and output to a data file that was later translated into a stress–strain curve.

3.2. Adiabatic heating

The deformation of the polymer generates heat. The general energy balance equation is classically given by

$$\rho(\theta)\cdot c_{p}(\theta)\cdot\dot{\theta}-\mathrm{div}(\Gamma(\theta)\cdot\mathrm{grad}(\theta))=\dot{q} \tag{31}$$

where $\rho(\theta)$ is the density, $c_{p}(\theta)$ is the specific heat, $\Gamma(\theta)$ is the thermal conductivity, and $\dot{q}$ is the rate of heat generation due only to plastic flow (Boyce et al., 1992; Arruda et al., 1995) and is equal to $[\mathrm{Trace}(\mathbf{T}^{*\prime}\mathbf{D}^{p})]$. The plastic work associated with the back stress is supposed to be stored as free energy in the material due to locked-in orientation. In our case, we neglect the effect of thermal conductivity since we will only simulate the mechanical response on a single element (homogeneous case). Besides, as a small simplification, the quantity $[\mathrm{Trace}(\mathbf{T}^{*\prime}\mathbf{D}^{p})]$ is assimilated to $[\tau\cdot\dot{\gamma}_{p}]$. The resulting energy balance equation is then given by

$$\dot{\theta}=\frac{\tau\cdot\dot{\gamma}_{p}}{\rho(\theta)\cdot c_{p}(\theta)} \tag{32}$$

4. Results and discussion

4.1. Simulated results

4.1.1. Influence of strain rate on the stress–strain curves

The influence of strain rate on the predicted true stress–true strain compression curves of PMMA and PC at 25 °C is reported in Fig. 5. Relative to the mechanical responses of PC, PMMA shows a strong influence of the strain rate on the yield stress and on the magnitude of the orientational hardening. At very high strain rates,

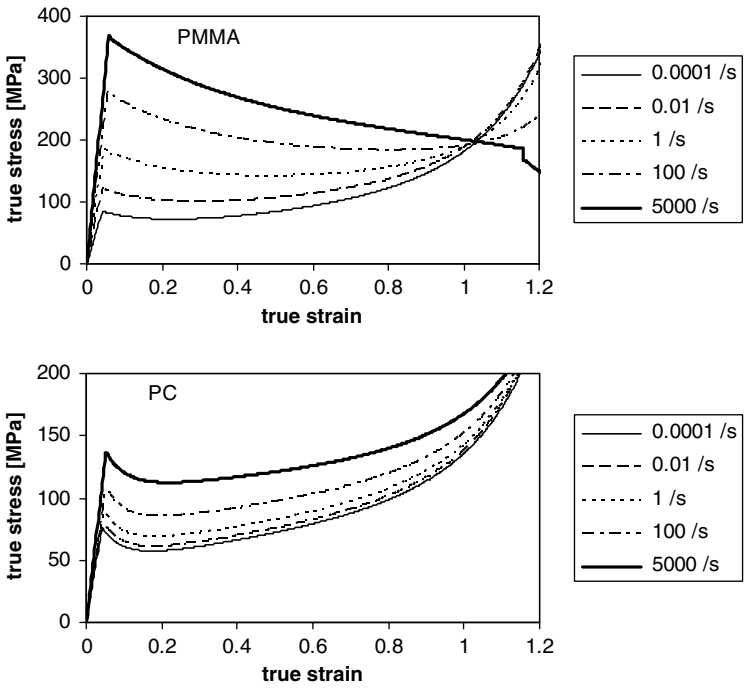

Fig. 5. Simulated results at a temperature of 25 °C for the compression stress of PMMA and PC. Influence of true strain rate.

PMMA does not exhibit any orientational hardening due to the rise of temperature resulting from adiabatic heating. The abrupt drop of the stress at a strain equal to about 1.1 on the stress–strain curve at the strain rate, $\dot{\varepsilon} = 5000\ s^{-1}$, is due to the transition from the glassy to the rubbery state of PMMA. In contrast, the high glass transition temperature of PC leads to less effect of the adiabatic heating on the orientational hardening. If the simulations for PC are conducted at a temperature closer to its T_g, a similar drop in the stress–strain curve would be observed. At low strain rate, the mechanical response of PC shows a weaker dependence on strain rate in comparison to PMMA. This effect can be explained by comparing the values of the secondary activation energies for these two materials.

4.1.2. Influence of temperature on the stress–strain curves

Fig. 6 illustrates the influence of temperature on the predicted true stress–true strain response under uniaxial compression for PMMA and PC. These simulations are conducted at a true strain rate, $\dot{\varepsilon} = 0.01\ s^{-1}$, to minimize the adiabatic heating effect. At low temperatures, the results are probably purely speculative according to a competition between yielding and brittle failure. This statement is particularly true for PMMA since this material exhibits a brittle behavior at low temperatures where the yield stress cannot be reached. The transition behavior across the glass transition temperature range from the glassy to rubbery states is predicted both for PMMA and PC.

4.1.3. Influence of the testing mode on the stress–strain curves

Fig. 7 presents a comparison between the evolutions of the mechanical response for different deformation states. The hardening response is very different in each test since the orientational hardening trend is related to the degrees of freedom of chains. The degree of freedom for chain alignment is higher for uniaxial compression, wherein the chains align in the radial direction of the compressed sample. In contrast, for uniaxial tension the degree of freedom is lower, wherein the chains align within the tensile direction. The hardening under plane strain compression is closer to that in tension because of the boundary conditions, where one of the macroscopic directions is constrained to zero strain. At low strains, the predicted yield points are different for different loading conditions. These are ranked in the following decreasing order: plane strain compression, uniaxial compression, simple shear, uniaxial tension. This result is an outcome of the hypothesis of the linear dependence of the yield stress on the hydrostatic pressure (see Eq. (2)).

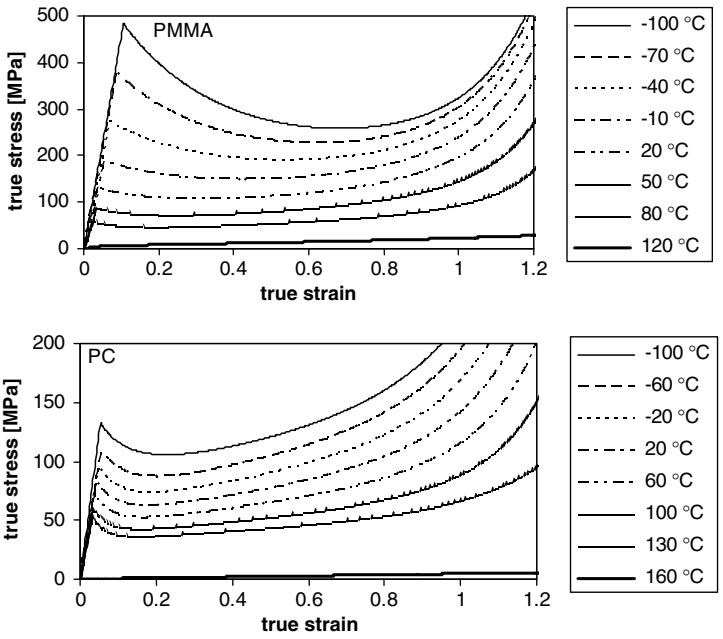

Fig. 6. Simulated results at a true strain rate of $0.01\ s^{-1}$ for the compression stress of PMMA and PC. Influence of temperature.

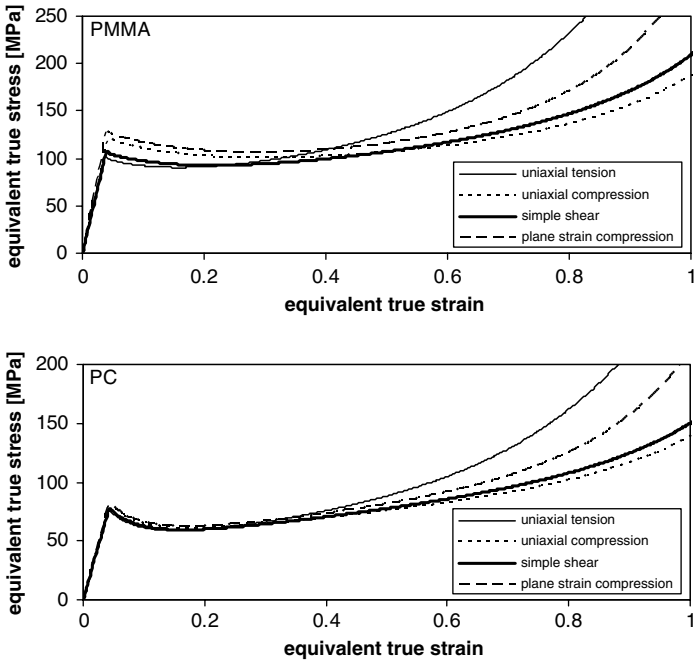

Fig. 7. Comparison between the simulated equivalent true stress–strain curves of PMMA, and PC for different deformation states. The simulations were run at a temperature of 25 °C and at a true strain rate of 0.01 s^{-1}.

4.2. Comparison with experimental results in compression

The modeling results are compared to experimental data in compression for PMMA and PC at different strain rates and temperatures. The model parameters are fitted for each polymer on the experimental data at a specified strain rate and temperature, and then the same parameters are used to predict the mechanical response for other temperatures and strain rates (see Figs. 8 and 9). The quasi-static uniaxial compression tests were conducted on a standard servohydraulic load frame, and the dynamic uniaxial compression tests were conducted using a 12.7 mm diameter split Hopkinson pressure bar (SHPB) setup. The details of these experimental procedures have been published previously elsewhere (Richeton et al., 2006).

The quasi-static tests were conducted at constant displacement rates. During the compression, the true strain rate increases slightly from its nominal value. Therefore, the numerical simulations were also conducted at constant engineering strain rates to avoid any discrepancy between the predicted curves and the experimental data at large strains.

In the case of dynamic testing, the compression tests and simulations were conducted at nearly constant true strain rate. However, the functionality limitation of the SHPB setup allows reaching large strains only for the high strain rates. In fact, the strain and strain rate in the SHPB testing are in a complex interaction. They depend on the striker bar length, the gun pressure (striker velocity), and the sample deformation behavior. Our experimental results show therefore an increasing amount of strain with the strain rate since we used the same striker bar length with different gun pressure. We note that larger strains at a lower strain rates could be achieved using a longer striker bar.

Subsequent figures are labeled with the temperature and strain rate shown on the top of each figure. Figs. 8 and 9 show good agreement between the experimental and simulated stress–strain curves. At small strains, the use of a temperature and rate dependent statistical model for the initial Young's modulus provides a correct description of the experimental data at high strain rates and in the rubbery region. The cooperative model, used as a flow rule, is able to capture the temperature and strain rate dependence of the compressive yield stress. Unfortunately, due to the lack of data in tension, it was not possible to determine the validity of the hydrostatic pressure effect on the yield stress. Relative to the stress–strain response of PC, the PMMA

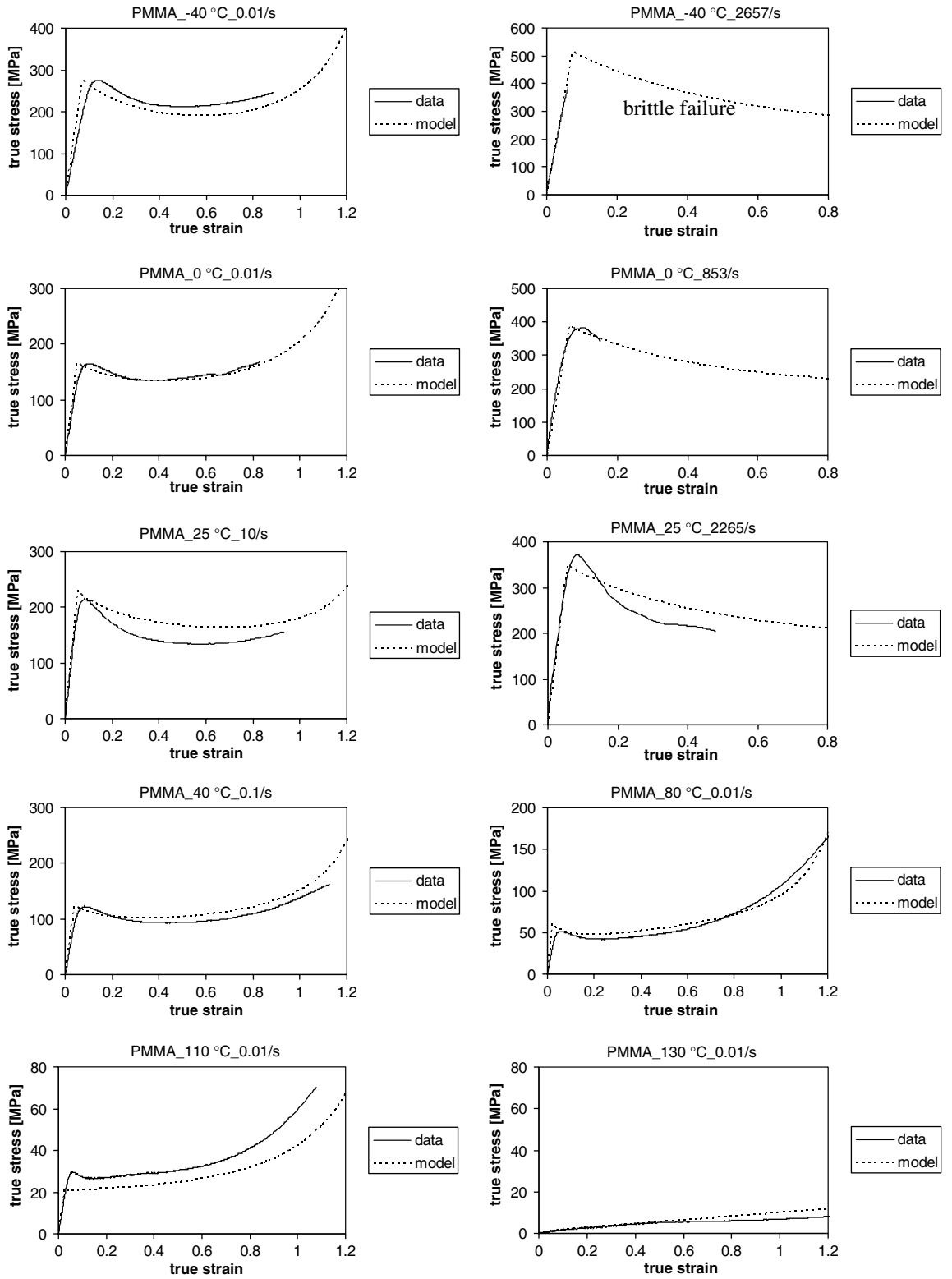

Fig. 8. Validation of the model for PMMA on a wide range of temperatures and strain rates. Quasi-static experiments and simulations were conducted at constant displacement rates whereas dynamic experiments and simulations were conducted at constant true strain rates.

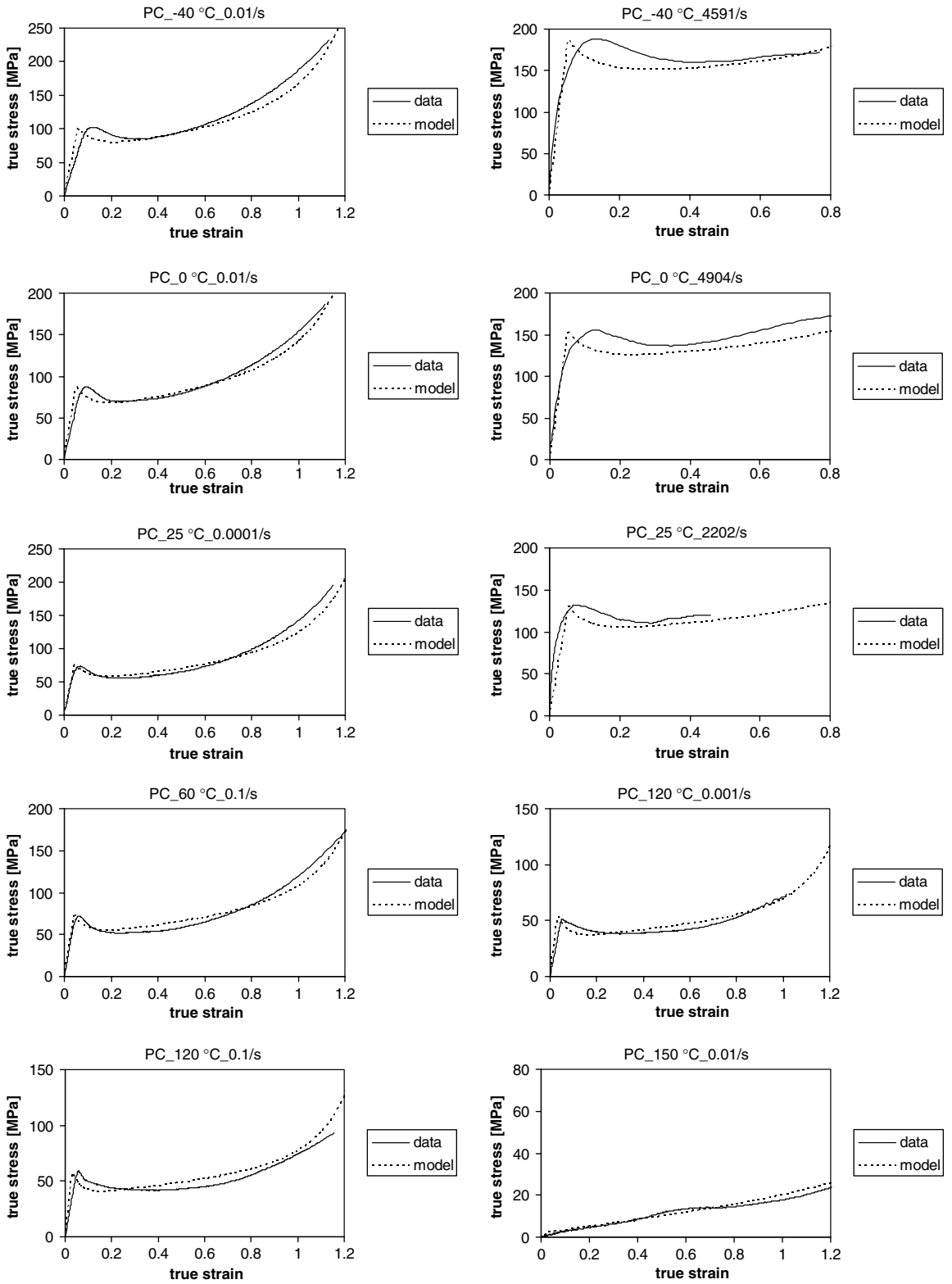

Fig. 9. Validation of the model for PC on a wide range of temperatures and strain rates. Quasi-static experiments and simulations were conducted at constant displacement rates whereas dynamic experiments and simulations were conducted at constant true strain rates.

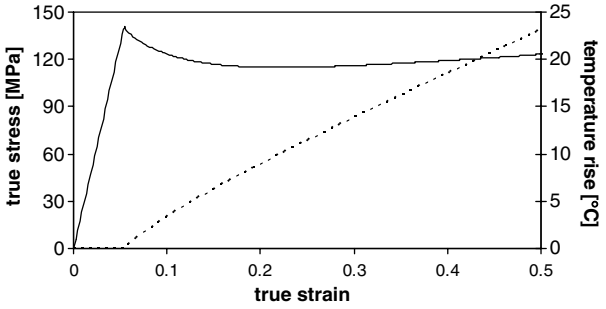

Fig. 10. True stress and temperature rise of PC plotted versus the true strain. In lines with the results of Rittel (1999), the test conditions were 25 °C and 6500 s^{-1}. The temperature rise is zero in the elastic region before presenting a quasi-linear increase after the yield point.

post-yield model predictions underestimate the experimental results at high strain rates. The main difficulty in the modeling of the post-yield lies in the fact that there is a competition between the strain softening associated with adiabatic heating and the orientational hardening. As it was noticed by Billon (2003), the self-heating of the polymer become significant above a strain rate of 0.01 s^{-1}.

Further, the adiabatic heating at very high strain rates is poorly described in our modeling. Experimental results of Rittel (1999) for the adiabatic heating at high strain rate, $\dot{\varepsilon} = 6500\ s^{-1}$, showed a step-like increase of temperature, whereas our predicted temperature presents nearly a linear increase with deformation (see Fig. 10). In the case of dynamic testing, Bjerke and Lambros (2002) and Bjerke et al. (2002) have shown that additional heat effects, such as the phenomena present during dynamic fracture, must be considered in the simulation to get a more accurate comparison with the experiments. However, this linear evolution of the temperature with deformation was experimentally validated for low and medium strain rates by Arruda et al. (1995).

5. Conclusions

A robust physically consistent constitutive model for the large inelastic deformation of amorphous polymers has been presented. In addition to being able to account for the effects of strain rate, temperature and hydrostatic pressure, this thermomechanical model can account for the possible change of the polymer from the glassy to the rubbery state due to adiabatic heating at very high strain rates. Intramolecular, as well as intermolecular, interactions under large elastic–inelastic behavior were considered for the mechanisms of deformation and hardening. The results from the implemented model were compared to experimental results, which in turn, were used to tune the proposed constitutive laws. Good agreement between the modeling and the experimental results was obtained for poly(methyl methacrylate) (PMMA) and polycarbonate (PC). This proposed model can be seen as a decisive step towards the development of advanced material constitutive models for the description of the mechanical response of thermoplastic polymers solicited under a wide range of temperatures, strain rates, and pressures.

Acknowledgments

The authors thank R.R. Adharapurapu from the *University of California, San Diego* for help with the quasi-static uniaxial compression testing. In addition, J. Richeton is grateful for the financial support of his Ph.D. thesis by the *French National Center for Scientific Research (CNRS)* and by the *Région Alsace*.

References

Argon, A.S., 1973. A theory for the low temperature plastic deformation of glassy polymers. Philosophical Magazine 28, 839–865.

Arruda, E.M., Boyce, M.C., 1993. Evolution of plastic anisotropy in amorphous polymers during finite straining. International Journal of Plasticity 9, 697–720.

Arruda, E.M., Boyce, M.C., Jayachandran, R., 1995. Effects of strain rate, temperature and thermomechanical coupling on the finite strain deformation of glassy polymers. Mechanics of Materials 19, 193–212.

Bauwens, J.C., Bauwens-Crowet, C., Homès, G., 1969. Tensile yield-stress behavior of poly(vinyl chloride) and polycarbonate in the glass transition region. Journal of Polymer Science: Part A-2 7, 1745–1754.

Bauwens, J.C., 1972. Relation between the compression yield stress and the mechanical loss peak of bisphenol-A-polycarbonate in the β transition range. Journal of Materials Science 7, 577–584.

Bauwens-Crowet, C., Bauwens, J.C., Homès, G., 1969. Tensile yield-stress behavior of glassy polymers. Journal of Polymer Science: Part A-2 7, 176–183.

Bauwens-Crowet, C., Bauwens, J.C., Homès, G., 1972. The temperature dependence of yield of polycarbonate in uniaxial compression and tensile tests. Journal of Materials Science 7, 176–183.

Bauwens-Crowet, C., 1973. The compression yield behaviour of polymethyl methacrylate over a wide range of temperatures and strain-rates. Journal of Materials Science 8, 968–979.

Bicerano, J., 1993. Prediction of Polymer Properties. Marcel Dekker Inc., New York.

Billon, N., 2003. Effet de couplage thermomécanique dans la caractérisation du comportement de polymères solides. Mécanique et Industries 4, 357–364.

Bjerke, T., Lambros, J., 2002. Heating during shearing and opening dominated dynamic fracture of polymers. Experimental Mechanics 42, 107–114.

Bjerke, T., Li, Z., Lambros, J., 2002. Role of plasticity in heat generation during high rate deformation and fracture of polycarbonate. International Journal of Plasticity 18, 549–567.

Boyce, M.C., Montagut, E.L., Argon, A.S., 1992. The effect of thermomechanical coupling on the cold drawing process of glassy polymers. Polymer Engineering and Science 32, 1073–1085.

Boyce, M.C., Parks, D.M., Argon, A.S., 1988. Large inelastic deformation of glassy polymers. Part I: Rate dependent constitutive model. Mechanics of Materials 7, 15–33.

Cady, C.M., Blumenthal, W.R., Gray III, G.T., Idar, D.J., 2003. Determining the constitutive response of polymeric materials as a function of temperature and strain rate. Journal de Physique IV 110, 27–32.

Cohen, A., 1991. A Padé approximant to the inverse Langevin function. Rheologica Acta 30, 270–273.

Dooling, P.J., Buckley, C.P., Rostami, S., Zahlan, N., 2002. Hot-drawing of poly(methyl methacrylate) and simulation using a glass–rubber constitutive model. Polymer 43, 2451–2465.

Edwards, S.F., Vilgis, T., 1986. The effect of entanglements in rubber elasticity. Polymer 27, 483–492.

Eyring, H., 1936. Viscosity, plasticity, and diffusion as examples of absolute reaction rates. Journal of Chemical Physics 4, 283–291.

Fotheringham, D., Cherry, B.W., 1976. Comment on "the compression yield behaviour of polymethyl methacrylate over a wide range of temperatures and strain-rates". Journal of Materials Science 11, 1368–1370.

G'Sell, C., Souami, A., 1997. Influence of crosslinking on the plastic behavior of amorphous polymers at large strains. Journal of Engineering Materials and Technology 119, 223–227.

Mahieux, C.A., Reifsnider, K.L., 2001. Property modeling across transition temperatures in polymers: a robust stiffness temperature model. Polymer 42, 3281–3291.

Mahieux, C.A., Reifsnider, K.L., 2002. Property modeling across transition temperatures in polymers: application to thermoplastic systems. Journal of Material Science 37, 911–920.

Meyer, K.H., Ferri, C., 1935. Sur l'élasticité du caoutchouc. Helvetica Chimica Acta 18, 570–589.

Mulliken, A.D., Boyce, M.C., 2006. Mechanics of the rate-dependent elastic–plastic deformation of glassy polymers from low to high strain rates. International Journal of Solids and Structures 43, 1331–1356.

Parks, D.M., Argon, A.S., Bagepalli, B., 1984. Large elastic–plastic deformation of glassy polymers. In: Technical Report MIT—Program in Polymer Science and Technology.

Richeton, J., Ahzi, S., Daridon, L., Rémond, Y., 2003. Modeling of strain rates and temperature effects on the yield behavior of amorphous polymers. Journal de Physique IV 110, 39–44.

Richeton, J., Ahzi, S., Daridon, L., Rémond, Y., 2005a. A formulation of the cooperative model for the yield stress of amorphous polymers for a wide range of strain rates and temperatures. Polymer 46, 6035–6043.

Richeton, J., Schlatter, G., Vecchio, K.S., Rémond, Y., Ahzi, S., 2005b. A unified model for stiffness modulus of amorphous polymers across transition temperatures and strain rates. Polymer 46, 8194–8201.

Richeton, J., Ahzi, S., Vecchio, K.S., Jiang, F.C., Adharapurapu, R.R., 2006. Influence of temperature and strain rate on the mechanical behavior of three amorphous polymers: characterization and modeling of the compressive yield stress. International Journal of Solids and Structures 43, 2318–2335.

Richeton, J., Ahzi, S., Daridon, L., in press. Thermodynamic investigation of yield-stress-models for amorphous polymers. Philosophical Magazine.

Rittel, D., 1999. On the conversion of plastic work to heat during high strain rate deformation of glassy polymers. Mechanics of Materials 31, 131–139.

Robertson, R.E., 1966. Theory for the plasticity of glassy polymers. The Journal of Chemical Physics 44, 3950–3956.

Sweeney, J., 1999. A comparison of three polymer network models in current use. Computational and Theoretical Polymer Science 9, 27–33.

Van Krevelen, D.W., 1990. Properties of Polymers, third ed. Elsevier, Amsterdam.

William, M.L., Landel, R.F., Ferry, J.D., 1955. The temperature dependence of relaxation mechanisms in amorphous polymers and other glass-forming liquids. Journal of the American Chemical Society 77, 3701–3707.